AGU PUBLICATIONS

JGR

Journal of Geophysical Research: Atmospheres

RESEARCH ARTICLE
10.1002/2013JD021344

Key Points:
- We investigate snow albedo evolution during the spring melt season
- The existing snow albedo parameterizations for LSMs overestimate snow albedo
- The introduced parameterization improves energy and water flux simulation

Correspondence to:
M. J. Malik,
malik14406@itc.nl

Citation:
Malik, M. J., R. van der Velde, Z. Vekerdy, and Z. Su (2014), Improving modeled snow albedo estimates during the spring melt season, *J. Geophys. Res. Atmos.*, *119*, 7311–7331, doi:10.1002/2013JD021344.

Received 12 DEC 2013
Accepted 29 MAY 2014
Accepted article online 2 JUN 2014
Published online 27 JUN 2014

Improving modeled snow albedo estimates during the spring melt season

M. Jahanzeb Malik[1,2], Rogier van der Velde[1], Zoltan Vekerdy[1], and Zhongbo Su[1]

[1]Faculty of Geo-Information Science and Earth Observation (ITC), University of Twente, Enschede, Netherlands, [2]Pakistan Space and Upper Atmosphere Research Commission (SUPARCO), Karachi, Pakistan

Abstract Snow albedo influences snow-covered land energy and water budgets and is thus an important variable for energy and water fluxes calculations. Here, we quantify the performance of the three existing snow albedo parameterizations under alpine, tundra, and prairie snow conditions when implemented in the Noah land surface model (LSM)—Noah's default and ones from the Biosphere-Atmosphere Transfer Scheme (BATS) and the Canadian Land Surface Scheme (CLASS) LSMs. The Noah LSM is forced with and its output is evaluated using in situ measurements from seven sites in U.S. and France. Comparison of the snow albedo simulations with the in situ measurements reveals that the three parameterizations overestimate snow albedo during springtime. An alternative snow albedo parameterization is introduced that adopts the shape of the variogram for the optically thick snowpacks and decreases the albedo further for optically thin conditions by mixing the snow with the land surface (background) albedo as a function of snow depth. In comparison with the in situ measurements, the new parameterization improves albedo simulation of the alpine and tundra snowpacks and positively impacts the simulation of snow depth, snowmelt rate, and upward shortwave radiation. An improved model performance with the variogram-shaped parameterization can, however, not be unambiguously detected for prairie snowpacks, which may be attributed to uncertainties associated with the simulation of snow density. An assessment of the model performance for the Upper Colorado River Basin highlights that with the variogram-shaped parameterization Noah simulates more evapotranspiration and larger runoff peaks in Spring, whereas the Summer runoff is lower.

1. Introduction

Snow cover dynamics are important for weather, climate, and hydrological studies via its control on the length of snow seasons, the timing and rate of snowmelt and streamflow, and the magnitude of energy and water fluxes at the land-atmosphere interface [*Barnett et al*., 2005; *Souma and Wang*, 2010]. Snow albedo and snow water equivalent (SWE) are the variables of a snowpack that affect land surface's energy and water budgets [*Barlage et al*., 2010; *Malik et al*., 2012]. The SWE defines the liquid water volume within the snowpack, whereas the snow albedo determines directly the reflection of shortwave solar radiation at the snow-atmosphere interface and thus the total incoming net radiation. Indirectly, the snow albedo affects also the snow mass because the melting rate largely depends on the total incoming net radiation. As such, the snow albedo forms the direct link between energy and (snow) mass budgets. Amelioration of the snow albedo simulation within models will, therefore, improve simulation of surface energy budget as well as snow mass.

On global and continental scales, the energy fluxes at the land-atmosphere interface defined by the snow albedo impact also the stratosphere and troposphere and thus climate. *Allen and Zender* [2010], *Fletcher et al*. [2009a, 2009b], and *Randall et al*. [1994] showed that the snow albedo feedback is the primary mechanism by which snow affects atmospheric circulation, especially during springtime, by altering the geopotential heights. Moreover, *Lynch et al*. [1998] and *Qu and Hall* [2006] demonstrated that the climate simulated by a regional climate model is sensitive to the choice of the snow albedo parameterization in the land surface model (LSM). On the other hand, many studies [e.g., *Feng et al*., 2008; *Koivusalo and Heikinheimo*, 1999; *Molotch and Bales*, 2006; *Xue et al*., 2003] have shown that improved snow albedo calculations contribute to the reliability of snow mass and melt simulations. Similarly, *Malik et al*. [2012] showed that improved snow albedo representation within the Noah LSM through assimilation of observations improves not only the simulation of snowpack properties but also the simulation of radiative fluxes. These findings highlight the importance of snow albedo for modeling various hydro-meteorological processes.

Snow albedo depends primarily on the grain size and is typically lower for snowpacks with larger grains [e.g., *Malik et al*., 2011; *Wiscombe and Warren*, 1980]. Over time, snow grains grow because of thawing and refreezing processes referred to as snow metamorphism. Spatially variable atmospheric forcings induce spatially variable metamorphism rates. Thus, the snow albedo varies over both space and time, which complicates snow albedo modeling. Within land surface (e.g., Noah, Biosphere-Atmosphere Transfer Scheme (BATS), Canadian Land Surface Scheme (CLASS), Variable Infiltration Capacity (VIC)) and hydrological (e.g., Distributed Hydrology Soil Vegetation Model) models, the snow albedo is commonly modeled as a function that decays with snow age. Although implementations of the snow albedo decay have improved hydro-meteorological simulations [*Livneh et al*., 2010], still uncertainties exist mainly due to the oversimplified handling of the complex snow albedo decay during the melt season where snowpacks disappear [*Picard et al*., 2012; *Zender*, 2012].

We explore an alternative snow albedo parameterization for LSMs through comparisons of offline simulations with observations for better characterization of the evolution of snow albedo during the melt season so as to improve the simulation of snow states and surface energy and water budgets as well. We investigate the snow albedo decay during springtime using in situ measurements collected under alpine, tundra, and prairie snowpack conditions and assess performance of four snow albedo parameterizations when implemented within the Noah LSM [*Ek et al*., 2003]. In addition to Noah's default option, a newly developed and two existing snow albedo parameterizations from BATS and CLASS are included in the analysis. The in situ measurements used for this study have been collected throughout the globe under various conditions and include five alpine sites, one tundra site, and two prairie sites. Data from four of the alpine and one of the prairie sites are from the 2002–2003 Cold Land Processes Field Experiment (CLPX) campaign in Colorado, U.S. Another alpine snow data set is from a French site located in the Chartreuse mountain range of the Rhone-Alps. The tundra snow data set has been collected in Alaska, U.S. as a part of the AmeriFlux network, and the second prairie snow data set has been acquired from the Tibetan Plateau. The eight snow data sets all comprise measurements of both land-surface and near-surface atmospheric variables and form, as such, a comprehensive platform for providing new insights into snow albedo decay processes and evaluating the performance of the existing and new parameterizations.

This paper is organized as follows. Sections 2 and 3 introduce the test sites and the in situ measurements, respectively. Section 4 describes the observed snow albedo evolution. Section 5 presents the relevant Noah LSM physics and snow albedo parameterizations. Section 6 presents assessment of the parameterizations and its impacts on snow depth and energy/mass flux simulations through a comparison of the Noah LSM simulations with the in situ measurements. Implications of the snow albedo parameterization at a large scale are discussed for the Upper Colorado River Basin (UCRB) in section 7. The conclusions are presented in section 8.

2. Study Sites

Measurements collected at eight sites under alpine, prairie, and tundra snow conditions are used for this investigation: six sites are situated in the U.S., one in France, and one on the Tibetan Plateau. Alpine snow represents deep snowpacks with snow grains ranging from fine to coarse, basal depth hoar (faceted ice crystals), and interspersed ice lenses. To the contrary, tundra and prairie snow are shallow. Tundra snow lives, however, longest and develops depth hoar and wind slabs due to cold winters. While prairie snow, despite being comparable with tundra snow in depth, is transient and sporadic and composed primarily of medium-grained snow with rare wind slabs and depth hoar. Table 1 provides a list of the eight sites along with basic geographic information.

Data sets from five sites were acquired in Colorado (U.S.) during the NASA-sponsored CLPX campaign conducted in the 2002–2003 winter season. The sites are named Buffalo Pass (RB), Spring Creek (RS), Walton Creek (RW), Fraser Alpine (FA), and Illinois River (NI) and are part of the Meso-cell Study Areas (MSAs) Rabbit Ears, Fraser, and North Park. The first letter of the site code in Table 1 refers to its corresponding MSA. The CLPX sites are located in a diverse landscape including broad glades, meadows, and grasslands. The NI site is situated in low rolling terrain, the sites RB, RS, and RW are located on mountain slopes, and the FA site resides on a mountain top. The differences in elevation create weather variability over small spatial and short temporal scales. The Fraser MSA is cooler than the two other MSAs mainly due to a higher elevation. Heavy

Table 1. List of the Study Sites Along With Their Geographic Information and Snowpack Conditions[a]

Site (Code)	Long. (Deg.)	Lat. (Deg.)	Alt. (m)	Country	Snow Cover Class
[b]Buffalo Pass (RB)	−106.678	40.534	3200	Colorado, US	Alpine
[b]Spring Creek (RS)	−106.758	40.529	2800	Colorado, US	Alpine
[b]Walton Creek (RW)	−106.646	40.400	2950	Colorado, US	Alpine
[b]Fraser Alpine (FA)	−105.861	39.848	3585	Colorado, US	Alpine
Col de Porte (CDP)	5.77	45.3	1325	Rhône-Alpes, France	Alpine
[b]Illinois River (NI)	−106.255	40.695	2475	Colorado, US	Prairie
Namco lake site (Namco)	90.988	30.774	4730	Tibetan Plateau, China	Prairie
Ivotuk (Ivo)	−155.748	68.487	568	Alaska, US	Tundra

[a]Coordinates are provided in latitude and longitude using the WGS 84 geodetic system.
[b]The first letter of the Colorado sites is from the Cold Land Processes Field Experiment Meso-cell Study Area (CLPX MSA), and the second letter is from the site name.

snowfall often occurs at Rabbit Ears because of orographic effects, which results in the deepest alpine snowpacks at the site (e.g., Buffalo Pass) with the highest elevation of the MSA in Colorado. On the other hand, North Park experiences relatively little snowfall because it is situated in a mountain shadow area. Additionally, wind and sublimation contribute to the distribution of the shallow snowpacks at North Park as is typical for prairie snow conditions. More information on CLPX can be found at http://www.nohrsc.nws.gov/~cline/clpx.html (accessed 4 December 2013).

The other alpine site is the Col de Porte (CDP) site located in a grassy meadow at an altitude of 1325 m in the Chartreuse mountain range, France. Meteo-France operates this site in collaboration with other institutions since 1959. Continuous snow cover from late fall (December) to early spring (April) and low wind speeds characterize the area. Snow drift is thus limited in the area, and snowpacks may reach depths up to 1.5 m.

Ivotuk (Ivo) is the tundra site located on the north slope of the Brooks Range in Alaska, U.S. The land cover of the site is open shrubland with little relief. The site is part of Ameriflux network supported by the U.S. Global Change Research program, which focuses on the observations of energy, water, and carbon fluxes. In this region, snow accumulation starts at the end of September and reaches a total depth of about 65 cm before the onset of the melting period in May. Mid-winter melt events are quite rare. In the open terrain, weathering effects (e.g., cold wind) on the snowpack are strong, creating stratified snowpacks with depth hoar and relict wind crusts.

The data set of albedo measurements from the Tibetan Plateau is collected near the Namco Lake at an elevation of about 4700 m, used only for confirming the albedo evolution observed at the other shallow snowpack sites (i.e., Ivo and NI). The Institute for Tibetan Plateau Research of the Chinese Academy of Sciences (ITP-CAS) operates a permanent meteorological station equipped with a 20 m planetary boundary layer tower about 100 m from the shores of the lake. The land cover in the direct periphery is dominated by grassland with very little relief, but situated 10 km toward the south is a mountain range with peaks above 6000 m. The snowpacks are shallow, transient, and intermittent as is typical for prairie snow type conditions. The detailed description of this site can be found on website http://www.namco.itpcas.ac.cn/introductionen.html (accessed 4 December 2013).

3. Data Sets

The data sets available for the sites, except for the Namco site, include measurements of atmospheric forcings and snow properties needed for running the Noah LSM and evaluating its simulations [*Elder and Goodbody*, 2004; *Elder et al*., 2009; *Morin et al*., 2012; *Oechel*, 2012]. The near-surface atmospheric forcing data set comprises the measurements of air temperature, air humidity, surface pressure, wind speed, precipitation, and downward short- and longwave radiations. The atmospheric variables were measured approximately 1.5 m above the maximum anticipated snow depth at time intervals of 10, 30, and 60 min for the CLPX sites, Ivo, and CDP sites, respectively. Surface and soil temperatures as well as soil moisture measurements are used for the model initialization. The meteorological towers were also equipped with instrumentation for measuring snow depths surface albedo, and upward shortwave radiations. These measurements together with snowmelt measurements for the CDP site are used in this investigation for assessing the model performance. Table 2 lists the instruments deployed at the sites along with their reported specifications.

Table 2. List of Instruments and Respective Measurements Taken at the Various Study Sites[a]

Variable	Instruments	Accuracy
Atmospheric pressure	a) Vaisala PTB101B	±6 mb
	b) Standard Meteo-France sensor	±6 mb
	c) LI-COR 7500	±1.5%
Air temperature	a) Vaisala HMP45C	±0.5°C
	b) PT 100/4 wires	±0.1°C
	c) Vaisala HMP45C	±0.5°C
Air relative humidity	a) Vaisala HMP45C	±3%
	b) Vaisala HMP 35DE	±5%
	c) Vaisala HMP45C	±3%
Wind speed and direction	a) R.M. Young wind monitor	±2% and ±5°
	b) Laumonier and Chauvin Arnoux Tavid 87	±1%
	c) R.M. Young wind monitor	±2% and ±5°
Shortwave radiation	a) Kipp & Zonen CNR1	±10%
	b) Kipp & Zonen CM14	±10%
	c) Kipp & Zonen CNR1	±10%
Longwave radiations	a) Kipp & Zonen CNR1	±10%
	b) Eppley PIR	±10%
	c) Kipp & Zonen CNR1	±10%
Precipitation	a) –	
	b) GEONOR and PG2000	±0.1%
	c) Texas Electronics	±1%
Snow depth	a) Judd ultrasonic depth sensor	±1 cm
	b) Ultra-sound depth gauge BEN	±1 cm
	c) Campbell Sci. SR50	±1 cm
Snowmelt	a) –	
	b) Lysimeter	
	c) –	
Soil moisture and temperature	a) Stevens Vitel Hydra Probe	±0.03 and 0.6°C
	b) PT 100/4 wires	±0.1°C
	c) T107 thermistor	±0.2°C
Surface temperature	a) Apogee IRTS-P5	±0.4°C
	b) Testo term Pyroterm	±1.0°C
	c) T107 thermistor	±0.2°C

[a]a), b), and c) are for the CLPX, CDP, and Ivo sites, respectively.

Precipitation, needed to force the LSM, was not measured at the CLPX sites. Therefore, the precipitation inputs are obtained from the North American Land Data Assimilation System (NLDAS) for the sites. The NLDAS-2 precipitation product [*Ek et al*., 2011; *Xia et al*., 2012] is an hourly merged radar-gauge product at 1/8th degree (~12.5 km) spatial resolution, which is widely used for research purposes [e.g., *Feng et al*., 2008].

4. Measured Snow Albedo Decay During Melting Period

Figure 1 shows the in situ measurements of snow albedo and snow depth made at four of the five alpine sites. Since the solar zenith angle affects snow albedo by altering penetration depth of solar insolation [*Wiscombe and Warren*, 1980], the values shown are the measurements taken around the local noontime +/−2 h. The fairly small daily albedo variations suggest that the measurements were mostly collected under cloud free conditions. The figure highlights the important features of albedo evolution during melt season common for all the alpine sites from the onset of melting. The most prominent features are that the albedo (i) drops to the minimum value of 0.45–0.5, (ii) stays around this value as long as the snowpack remains optically thick (i.e., snow depth ≥50 cm for the springtime melting snowpack), and (iii) starts to decrease again when snowpack becomes optically thin (i.e., snow depth <50 cm for the springtime melting snowpack) because from that instant on the albedo is no longer a function of snow albedo alone and also depends on background albedo (viz. albedo of land surface beneath the snowpack). *Cline* [1997b] has made similar observations regarding the albedo decay during the melting periods of the 1993–1994 and 1995–1996 snow seasons at the Niwot Long-Term Ecological Research site in the Colorado Front Range.

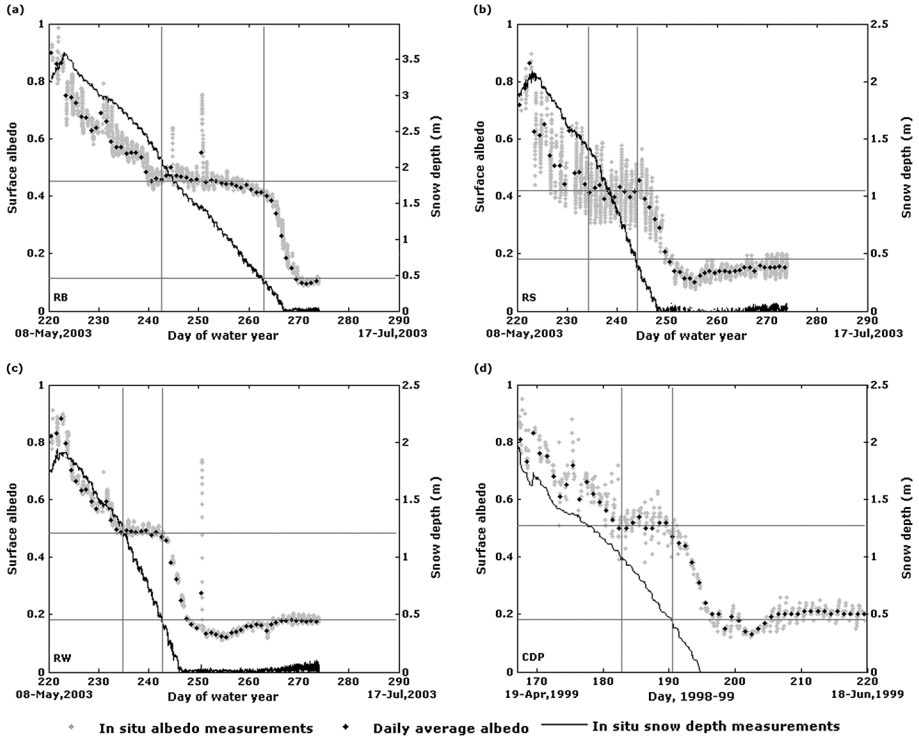

Figure 1. In situ snow albedo and depth measurements for the alpine snow sites. Figures 1a, 1b, 1c, and 1d show the measurements at Buffalo Pass (RB), Spring Creek (RS), Walton Creek (RW), and Col de Porte (CDP) sites, respectively. Measurements for the Fraser Alpine (FA) site reveal similar patterns and are not shown for brevity. The left-hand and right-hand vertical lines highlight the instants when the albedo reaches the minimum value of optically thick snowpack and when the snowpack becomes optically thin, respectively. The top horizontal line indicates the minimum albedo value of optically thick snowpacks, and the bottom horizontal line is the depth up to the melting snowpack remains optically thick.

Figure 2 presents the albedo evolution for the tundra and two prairie sites. Again, the values shown are the measurements taken around the local noontime +/−2 h. As prairie and tundra snowpacks are shallow (i.e., maximum snow depth ~50 cm [*Sturm et al*., 1995]), the melting makes the snowpack instantly optically thin. Consequently, the background albedo affects the measured albedo at the top of the snowpack from the start of melt. Further ablation gradually decreases the albedo to the value of the lower background albedo regardless of the snow cover type. In other words, the albedo decay of prairie and tundra snowpacks resembles the alpine snowpack from the instant when the alpine snowpack becomes optically thin.

5. The Noah LSM

5.1. Snowpack Physics

For this investigation, we make use of the Noah LSM version 3.4 that treats snowpack as a single layer for which it simulates the snowpack properties: e.g., SWE, albedo, density, depth, and snow cover fraction. Noah adopts an energy balance (equation (1)) approach to compute the melting rate (equation (2)) and simulate the SWE (equation (3)) and snow depth (equation (4)) according to the following equations,

$$Q_{net} = Q_{SW} + Q_{LW} + Q_h + Q_l + Q_g + Q_a \tag{1}$$

$$M = {}^{Q_{net}}\!/_{(\rho_w\, L_f)} \tag{2}$$

$$\Delta\mathrm{SWE} = P \pm E - M;\ \textit{where}\ E = {}^{Q_l}\!/_{L_v\,\rho_w} \tag{3}$$

$$\Delta d = \Delta SWE/_{\rho_{snow}} \tag{4}$$

where Q_{net} is the net energy available to melt or refreeze the snowpack [W/m^2], Q_{SW} and Q_{LW} are the net short- and longwave radiation fluxes at the surface of the snowpack [W/m^2], Q_h is the sensible heat flux [W/m^2],

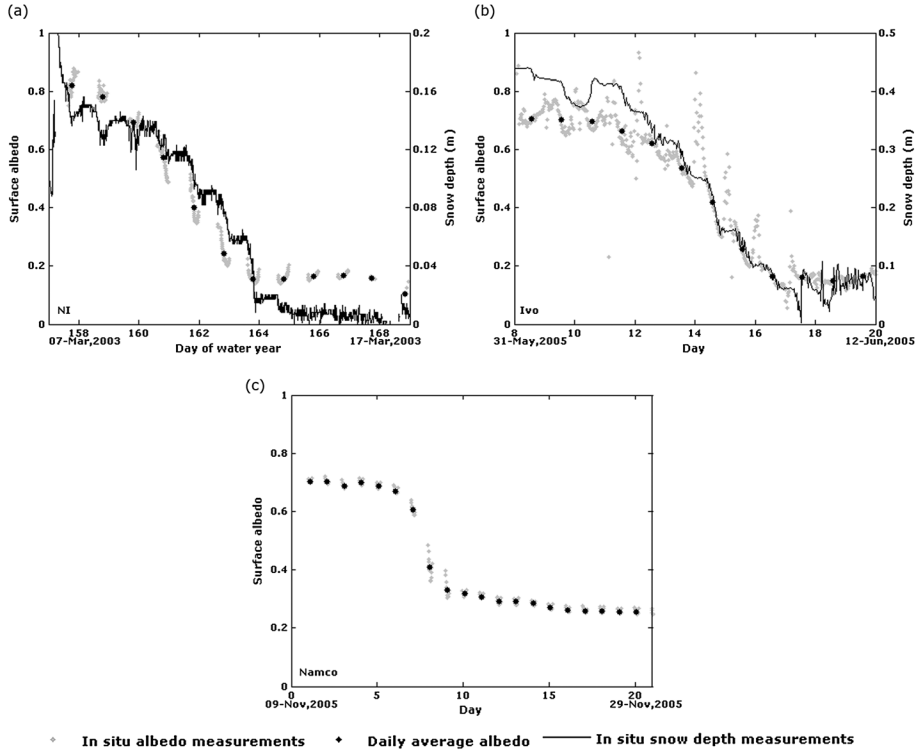

Figure 2. In situ measurements of snow albedo and snow depth for the prairie (Illinois River (NI) and Namco) and tundra (Ivotuk (Ivo)) sites. Figures 2a, 2b, and 2c show the measurements for the NI, Ivo, and Namco sites, respectively.

Q_l is the latent heat flux [W/m^2], Q_g is the ground heat flux [W/m^2], Q_a is the external energy source received by the snowpack (e.g., rain) [W/m^2], M is the melt rate [m/s], ρ_w is the liquid water density [kg/m^3], L_f is the latent heat of fusion [J/kg], P is the precipitation [m/s], E is the vapor exchange due to sublimation or evaporation and condensation [m/s], L_v is the latent heat of vaporization or sublimation [J/kg], d is the snow depth [m], and ρ_{snow} is the snowpack's density [kg/m^3].

The net shortwave radiation term (Q_{SW}) is calculated as follows,

$$Q_{SW} = Q_{SW\downarrow}(1 - \alpha_{snow}) \tag{5}$$

$$\alpha_{snow} = \alpha_{max} A^{t^B} \tag{6}$$

where $Q_{SW\downarrow}$ is the downward solar radiation [W/m^2], α_{snow} is broadband snow albedo, α_{max} is the broadband albedo of fresh snow, t is the time since the last snowfall, and A and B are constants set, respectively, to 0.94 and 0.58 during accumulation, and to 0.82 and 0.46 during ablation [*Cherkauer et al.*, 2003; *Livneh et al.*, 2010; *U.S. Army Corps Of Engineers*, 1956; *Wigmosta et al.*, 1994].

The magnitude and relative importance of each energy component to alter energy budget (equation (1)) and snow mass (equation (2)) vary depending on the site characteristics (i.e., land cover and topography) and the weather conditions. During springtime, however, the net shortwave radiation (Q_{SW}) dominates the energy balance and is thus the force driving snowmelt when the snowpack reaches temperature above freezing point, especially at the alpine, mid-latitude open, and lodge pole canopy sites [*Cline*, 1997a; *Marks and Dozier*, 1992; *Marks et al.*, 2008; *Meiman et al.*, 1971]. Therefore, accurate snow albedo characterization within models is crucial not only for a reliable simulation of snow states but also for defining the upwelling shortwave radiation ($Q_{SW\uparrow} = \alpha_{snow}\, Q_{SW\downarrow}$) part of both the land surface and atmospheric energy budgets.

Due to the deficiencies in the simulation of snow processes with earlier versions of Noah (i.e., version 2.7 [*Pan et al.*, 2003; *Sheffield et al.*, 2003]), *Barlage et al.* [2010]and *Livneh et al.* [2010]recently improved the associated model physics including the snow albedo parameterization. The snow albedo parameterization has been changed from a constant albedo value to the time-varying formulation of equation (6). This a

parameterization that exponentially decays the snow albedo as a function of snow age, which is intended to mimic the effect of growing snow grains on the albedo [*Wiscombe and Warren*, 1980].

By default, the Noah LSM simulates the snow cover fraction (SCF) as a function of the SWE that affects the albedo at scale of a grid cell. However, this does not affect the snow simulations because the snow processes are only calculated over portion of the grid cell covered by snow.

5.2. Snow Albedo Parameterizations

Along with the new default snow albedo parameterization of Noah [*Livneh et al*., 2010], two other existing and one new parameterizations have been implemented in the Noah model and included in the evaluation. The two existing parameterizations originate from the BATS and CLASS LSMs, and the newly introduced parameterization adopts the structure of a semi-variogram to describe the albedo decay noted among the measurements. All three are briefly described below.

The BATS parameterization [*Anderson*, 1976; *Dickinson et al*., 1993] computes snow albedo (α_{snow}) as a combination of the visible (α_V; wavelengths: 0.3–0.75 μm) and infrared (α_{IR}; wavelengths: 0.75–2.5 μm) albedos, which are functions of both snow age (f_{age}) and solar zenith angle ($f_{Z,s}$) according to,

$$\alpha_{V,dif.} = \alpha_{V0}\left(1 - C_S f_{age}\right) \tag{7a}$$

$$\alpha_{IR,dif.} = \alpha_{IR0}\left(1 - C_N f_{age}\right) \tag{7b}$$

$$\alpha_V = \alpha_{V,dif.} + 0.4 f_{Z,s}\left(1 - \alpha_{V,dif.}\right) \tag{7c}$$

$$\alpha_{IR} = \alpha_{IR,dif.} + 0.4 f_{Z,s}\left(1 - \alpha_{IR,dif.}\right) \tag{7d}$$

$$\alpha_{snow} = 0.5\left(\alpha_V + \alpha_{IR}\right) \tag{7e}$$

where subscripts *V*, *IR*, and *dif*. stand for the visible, infrared, and diffuse components of the broadband albedo, respectively; α_{V0} and α_{IR0} are visible and infrared albedos of new snow and are set, respectively, to 0.95 and 0.65; and constants C_S and C_N are taken 0.2 and 0.5. The snow age factor (f_{age}) includes the effects of snowpack metamorphism and impurities as follows,

$$r_1 = exp\left[5000\left(\frac{1}{273.16} - \frac{1}{T_{g1}}\right)\right] \tag{8a}$$

$$r_2 = (r_1)^{10} \le 1 \tag{8b}$$

$$r_3 = \begin{cases} 0.01 \text{ over Antartica} \\ 0.3 \text{ elsewhere} \end{cases} \tag{8c}$$

$$\Delta\tau_s = (r_1 + r_2 + r_3)^{\Delta t}/_{\tau_0}. \tag{8d}$$

$$f_{age} = {}^{\tau_s}/_{(1+\tau_s)} \tag{8e}$$

where r_1 represents the effect of grain growth due to vapor diffusion, r_2 represents the effect of (nearly) freezing meltwater, r_3 is for the effect of dirt and soot, $\Delta\tau_s$ is the change in snow age in time Δt, and T_{g1} is the snow surface temperature [K]. The solar zenith angle (Z) effect on the albedo is computed as,

$$f_{Z,s} = \frac{1}{b}\left[\frac{1+b}{1+2b\ \cos Z} - 1\right],\ f_{Z,s} = 0\ if\ \cos Z > 0.5;\ b = 2.0 \tag{9}$$

where $f_{Z,s}$ is the solar zenith angle correction factor, and b is an experimentally determined parameter and set to 2 in BATS.

The CLASS parameterization [*Verseghy*, 1991] simply decreases snow albedo in time according to,

$$\alpha_{snow\,n} = \alpha_{snow\,min} + \left(\alpha_{snow\,n-1} - \alpha_{snow\,min}\right) exp^{-\beta\Delta t/3600}. \tag{10}$$

where α_{snown} and $\alpha_{snown-1}$ are snow albedos at n and $n-1$ time steps at Δt time interval [s], $\alpha_{snowmin}$ is the minimum snow albedo and set to 0.55, and β is the decay factor set to 0.01 (h^{-1}). The factor 1/3600 s in the exponent is included to convert the units.

The newly developed parameterization adopts for the melting period the shape of a circular semi-variogram to characterize the snow albedo decay noted in Figure 1 and decays the albedo further as the snowpack

Table 3. Parameter Sets for Four Snow Albedo Parameterizations Calibrated Using Measurements Collected Under Alpine Conditions During Springtime Snowmelt

		Noah's Default			Biosphere-Atmosphere Transfer Scheme (BATS)		
Sites	Calibration Periods	A	B	Root Mean Squared Error (RMSE)	C_S	C_N	RMSE
RB	3 May, 03 to 16 Jun, 03	0.93	0.58	0.075	0.9	1.1	0.077
RS	1 May, 03 to 31 May, 03	0.90	0.54	0.095	1.0	1.2	0.086
RW	3 May, 03 to 28 May, 03	0.94	0.66	0.082	0.8	1.1	0.092
FA	1 May, 03 to 23 May, 03	0.94	0.66	0.057	0.8	1.0	0.062
CDP	16 Apr, 99 to 8 May, 99	0.90	0.50	0.038	1.0	1.2	0.032
All site average		0.92	0.59		0.90	1.12	
		Canadian Land Surface Scheme (CLASS)			VAS		
		$\alpha_{snow\min}$	β	RMSE	a	c	RMSE
RB	3 May, 03 to 16 Jun, 03	0.55	0.004	0.096	25	0.44	0.050
RS	1 May, 03 to 31 May, 03	0.45	0.004	0.090	20	0.43	0.067
RW	3 May, 03 to 28 May, 03	0.45	0.003	0.076	20	0.45	0.046
FA	1 May, 03 to 23 May, 03	0.50	0.005	0.068	23	0.43	0.045
CDP	16 Apr, 99 to 8 May, 99	0.50	0.005	0.038	22	0.48	0.035
All site average		0.49	0.004		22	0.45	

becomes optically thin. Hereafter referred to as the VAriogram-Shaped (VAS) paramerization. The semi-variogram part of the parameterization is formulated as follows,

$$\alpha_{snow}(h) = \begin{cases} c\left\{1 - \frac{2}{\pi}\cos^{-1}\left(\frac{h}{a}\right) + \frac{2h}{\pi a}\sqrt{1 - \frac{h^2}{a^2}}\right\}, & h \le a \\ c, & h > a \end{cases} \tag{11}$$

Within the definition of the semi-variogram, h is the lag distance, c is the sill, and a is the range. In the context of the snow albedo decay, h represents the time since the onset of melting starting when an air temperature >274 K is reached as in previous studies [Cherkauer et al., 2003; Wigmosta et al., 1994]. This accommodates for the isothermal state of snowpacks at 273 K (0°C). The value c is the minimum snow albedo, and a is the time from the start of melt ($h = 0$) needed for an optically thick snowpack to reach the minimum snow albedo and hence defines snow albedo evolution rate.

When the snowpack becomes optically thin, the influence of background albedo (α_{bg}) on snow albedo is accounted for as a function of snow depth (d),

$$\alpha_{snow} = (d/0.5)^2\left(\alpha_{snow}(h) - \alpha_{bg}\right) + \alpha_{bg};\ \text{if } d < 0.5 \tag{12}$$

5.3. Calibration of Snow Albedo Parameterizations

For each of the four snow albedo parameterizations described above, the maximum snow albedo value (albedo of fresh snow) is set to 0.85, and two parameters are automatically calibrated using the quasi Newtonian Broyden-Fletcher-Goldfarb-Shanno (BFGS) algorithm [*Broyden*, 1970; *Fletcher*, 1970; *Goldfarb*, 1970; *Shanno*, 1970] for minimizing the Root Mean Squared Error (RMSE) calculated between the measured and computed snow albedo for each of the calibration periods monitored at the alpine test sites listed in Table 3. The episodes selected for calibration cover the complete snow albedo evolution of deep snowpacks from the maximum to the minimum snow albedo. Hence, the calibration periods capture the characteristic features of the snow albedo decay, which ensures a robust calibration of the snow albedo parameterizations.

Table 3 reports for each parameterization and site on the calibration periods employed for the calibration, the achieved errors, and the calibrated parameters. From Table 3, it is deduced that on average the RMSEs obtained with the Noah, CLASS, and BATS snow albedo parameterizations range from 0.069 to 0.074. A slightly improved performance is noted for the VAS parameterization with a RMSE reduction of 40–50% to a value of 0.049. Hence, it can be concluded that the VAS parameterization represents the snow albedo evolution during springtime best.

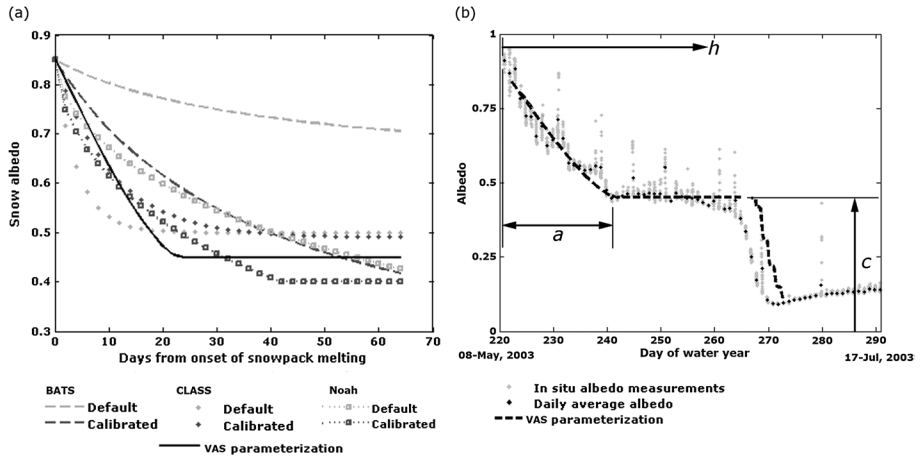

Figure 3. Behavior of snow albedo parameterizations as a function of time since the onset of snowmelt. Figure 3a shows the parameterizations with default and calibrated parameter sets. Figure 3b illustrates the interpretation of parameters of the VAS parameterization using the measurements of the RB site as an example.

Figure 3a shows curves of the existing (default and calibrated) and the VAS snow albedo parameterizations and illustrates the differences between snow albedo parameterizations. Figure 3b demarcates the VAS parameters and shows their role in representing the measured snow albedo evolution of alpine snowpacks during the snowmelt season. The sharp snow albedo decay from the onset of melting toward the minimum snow albedo and its further decay after the snowpack becomes optically thin are two features present within the measurements that are not captured by the existing parameterizations but are taken into consideration by the VAS parameterization. The snow albedo evolution of prairie and tundra snowpacks is approximated from the instant when the alpine snow albedo drops below 0.45 (Figure 3b).

To analyze the sensitivity of the VAS parameterization to its parameters, each parameter was varied over the physically plausible range of the parameter (e.g., 20–30 days for *a*, and 0.4–0.5 for *c*). The resulting change in albedo with respect to the reference (i.e., RB site in this case) is calculated as RMSE. The results are plotted in Figure 4 and show that the parameterization is more sensitive to *c* than *a*. Further, it shows that +/−10% change from the true *c* results in a 6% over-/under-estimation of snow albedo. In contrast, changes up to 20% in *a* result in a mere 3% variation in snow albedo estimation with the parameterization.

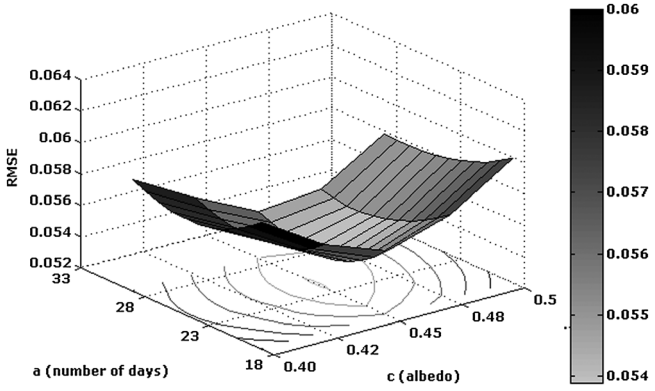

Figure 4. Root Mean Squared Error computed between measurements collected at the RB site and calculation with the VAriogram-Shaped (VAS) parameterization with *a* values ranging from 20 to 30 days and *c* (minimum snow albedo) values from 0.4 to 0.5 as indication for parameterization's sensitivity.

6. Noah Simulations

Noah was initialized using the measured land-surface states and driven at a 10 min interval using meteorological forcings measured at the seven sites. The parameters of each snow albedo parameterization are taken as the average of the five alpine sites' calibrated sets (see all site average in Table 3). Table 4 provides the initial values of the key land-surface states and the duration of the simulations for each site.

6.1. Snow Albedo

Figure 5 shows snow albedo simulations for the alpine sites using the four parameterizations. The

Table 4. List of Land Surface States Used as Model Initialization and Duration of Model Runs

Site	SWE (m)	Snow Depth (m)	Surface Temperature (K)	Soil Moisture[a] (m^3/m^3)	Soil Temperature[a] (K)	Start Date	End Date
RB	1.0	3.0	268	0.4,0.5,0.52	274,274.5,275	30-Mar-03	30-Jun-03
RS	0.63	1.8	269	0.2,0.22,0.25	274,274.5,275	30-Mar-03	20-Jun-03
RW	0.65	2.0	270	0.25,0.2,0.18	274,274.5,275	30-Mar-03	20-Jun-03
FA	0.45	1.7	269	*0.29,0.24,0.22*	*267,268,269*	26-Mar-03	20-Jun-03
CDP	0.6	1.58	267	*0.32,0.32,0.3*	273,274.5,275	28-Feb-99	11-Jun-99
NI	0	0	271	0.06,0.1,0.12	272,272.5,273	20-Feb-03	18-Mar-03
Ivo	0.21	0.65	269	*0.15,0.23,0.20*	271,271.6,272	24-May-05	15-Jun-05

[a]Comma separates values of soil moisture and temperature are for the first, second, and third soil layers. *Italics values are taken from Global Land Data Assimilation System (GLDAS) (for Ivo and CDP) and North American Land Data Assimilation System (NLDAS) (for FA). Soil moisture and temperature measurements are made for the three soil layers; the values of the third layer are repeated for the fourth layer.*

Noah, BATS, and CLASS parameterizations fail to capture accurately the features of albedo evolution throughout the melting period highlighted in section 4. For all the sites, these parameterizations overestimate snow albedo, which contributes to a prolonged presence of snowpacks. The performance of the new parameterization appears to be much better as is expected based on the results presented in section 5.3. Further, it should be noted that although only observations from second half of the snow season are used for calibration, the obtained parameters are not exclusively valid for this season as also episodes with an increase in snow depth and albedo occur in the selected simulation periods.

An additional benefit of the VAS parameterization over the others is its ability to adapt to local conditions (e.g., air temperature). For instance, the observed duration of the snow albedo decay (i.e., *a* parameter) can be deduced directly from albedo measurements (see Figure 1). Hence, the VAS parameterization offers also the opportunity to derive its parameter values from external snow albedo data sets—such as, from ground measurements [e.g., *Elder and Goodbody*, 2004; *Elder et al*., 2009; *Morin et al*., 2012; *Oechel*, 2012] or from satellite observations [e.g., *Klein and Stroeve*, 2002; *Liang et al*., 2005; *Malik et al*., 2011].

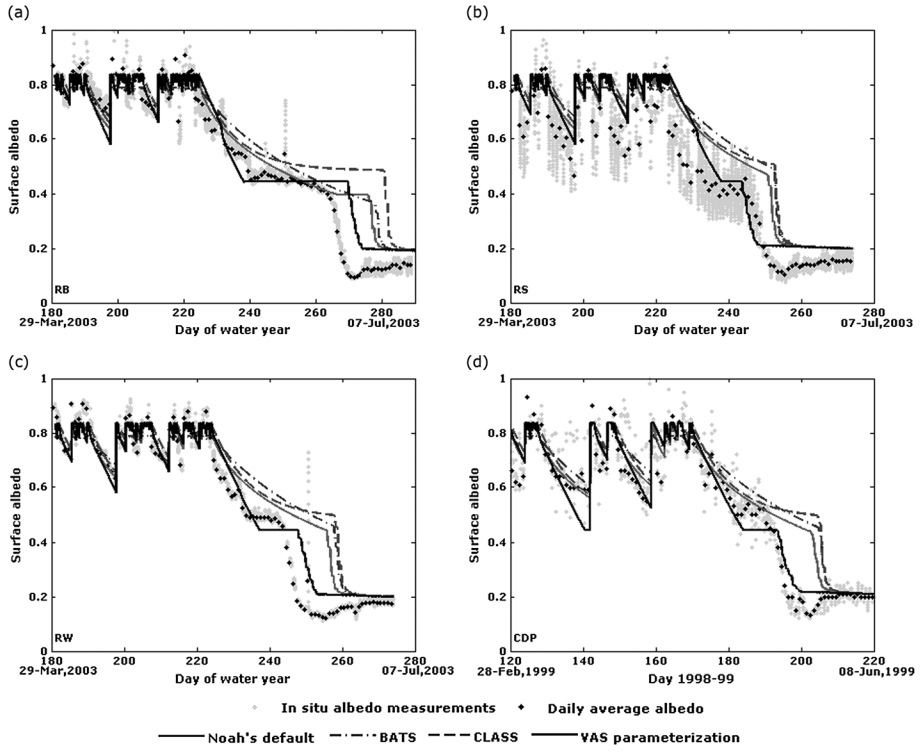

Figure 5. Evolution of observed and simulated snow albedo for the alpine sites. Figures 5a, 5b, 5c, and 5d are for RB, RS, RW, and CDP sites, respectively.

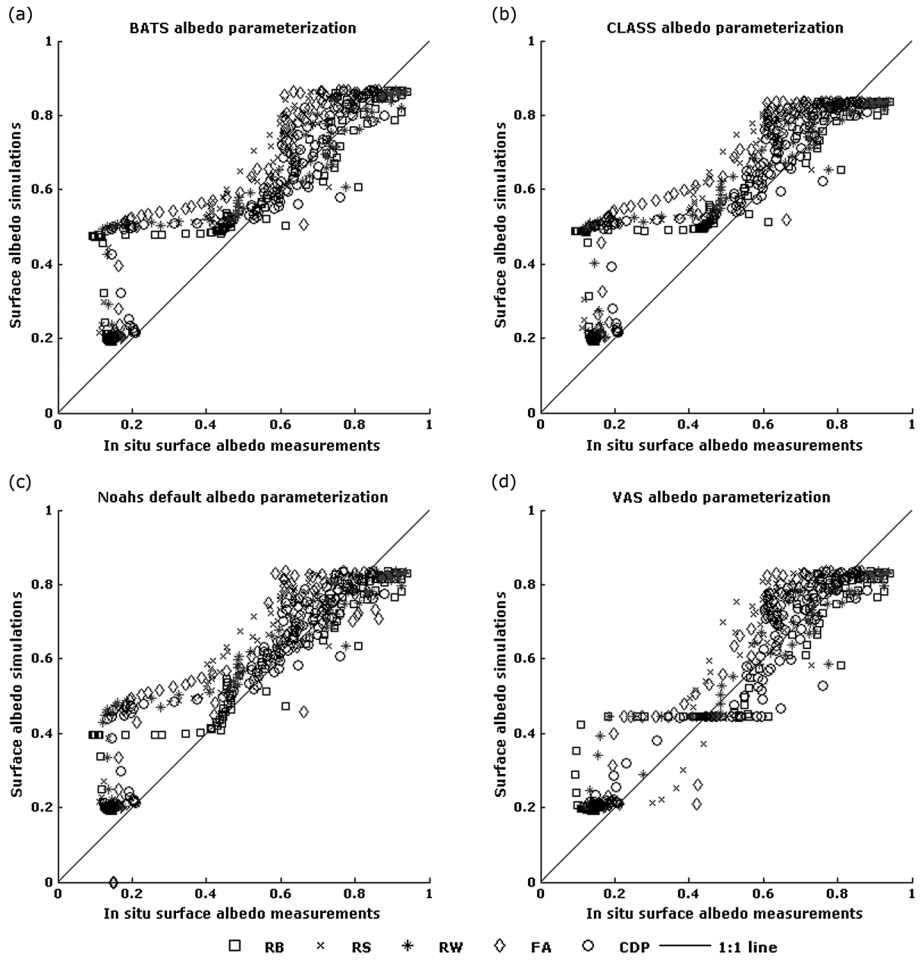

Figure 6. Scatterplots of snow albedo simulations versus in situ measurements for alpine snow conditions: (a) Biosphere-Atmosphere Transfer Scheme (BATS), (b) Canadian Land Surface Scheme (CLASS), (c) Noah's default parameterization, and (d) VAS parameterization.

Figure 6 compares the snow albedo simulations with the in situ measurements from the five alpine sites, and Table 5 provides overall error statistics (i.e., mean error (ME), mean absolute error (MAE), RMSE) of the comparisons. The error statistics and the correlation coefficients (i.e., *r*) indicate that the snow albedo simulations with the VAS parameterization best match the measurements. The results with the VAS parameterization are significantly better at 95% confidence level than the BATS and CLASS snow albedo parameterizations. However, the VAS parameterization simulations are not significantly better than the albedo simulations with the Noah's default snow albedo parameterization but yield, nevertheless, improvements in both the error statistics and correlation. This suggests that the VAS parameterization can better approximate albedo evolution during the melt season within Noah simulations.

Table 5. Error Statistics of the Noah Snow Albedo Simulations for the Alpine Sites[a]

	Noah	BATS	CLASS	VAS
r	+0.909	+0.908	+0.901	+0.923
Mean error (ME)	+0.044	+0.06	+0.074	+0.019
Mean absolute error (MAE)	0.079	0.083	0.095	0.068
RMSE	0.105	0.112	0.125	0.088
p-value[b]	0.136	0.022	0.001	Reference

[a]The temporal autocorrelation is corrected for by averaging over the correlation length of 10 days resulting in sample sizes of 48 values.
[b]*p*-values are derived using the Wilcoxon test, which is more conservative than *t* test.

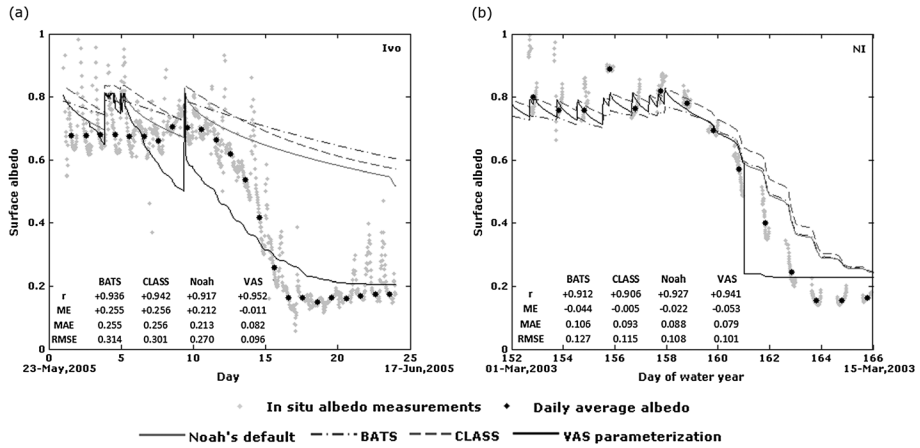

Figure 7. Evolution of observed and simulated snow albedo for the tundra (a, Ivo site) and prairie (b, NI site) snow conditions.

Figure 6 also shows that the major differences between the parameterizations are the rate, viz. slope of the scatterplot points, and extent, viz. range of simulated snow albedo, of the simulated albedo evolution. The CLASS parameterization produces snow albedos with the lowest extent and rate (almost 33°) and thus overestimate snow albedo with the largest ME. With Noah's default and the BATS parameterizations, simulations agree better with the measurements as compared to the CLASS simulations, but they produce a smaller snow albedo evolution rate (almost 35° and 37° for BATS and Noah, respectively) than the measured rate (1:1 line; i.e., 45°). The Noah model with the VAS parameterization produces more accurate extent and evolution rate (almost 42°) and performs the best for the alpine sites under evaluation.

For all the parameterizations, the largest uncertainties are observed as the snowpack becomes optically thin. In contrast to the existing ones, the VAS parameterization is accommodated for optically thin snowpacks. Nevertheless, discrepancies between the simulations and measurements are still observed. The VAS parameterization overestimates albedo due to late detection of the instant when the snowpack becomes optically thin (Figure 5). Two reasons explain this delayed detection: (i) uncertainties in overall energy balance at the snowpacks' surface (see equation (1)) and (ii) uncertainties related to the density calculations of the snowpack (see equation (4)). Density impacts the albedo evolution of optically thin snowpacks via the depth calculations (equation (4) affects equation (12)) and thus on the decision whether a snowpack is optically thick or thin. Therefore, the VAS parameterization's effectiveness to detect the instant when the snowpack becomes optically thin depends on density estimates also (Figures 5a and 5c), which are simulated differently in Noah and other LSMs.

The performance of the albedo parameterizations for the tundra and prairie sites is comparable to that of the alpine sites (Figures 7a and 7b); i.e., Noah's default snow albedo parameterization and the VAS parameterization are better than the BATS and CLASS snow albedo parameterizations. However, the VAS parameterization suffers from uncertainties in the snow density simulations, as is discussed above for the alpine sites. The uncertain density simulation causes uncertain snow depth simulations that affect the influence of the background albedo on the snow albedo evolution (equation (12)).

6.2. Snow Depth

Figure 8 illustrates the impact of the snow albedo parameterization on the snow depth by comparing for alpine snow conditions the simulations with in situ measurements. Associated error statistics are listed in Table 6.

The different snow albedo parameterizations alter snow depletion rate and affect thus the snow depth simulation. From the in situ snow depth measurements, it can be deduced that the depletion rates at the sites RB, RS, and RW are during the melt season on average 7.2, 8.2, and 7.9 cm/day, respectively (see Figure 1). Regardless of the employed snow albedo parameterization, the simulated snow depletion rates are lower as compared to the measured rates. Therefore, the simulated duration of snowpacks is longer than in reality as can be seen in Figure 8 for alpine and Figure 9a for tundra snow conditions. Nevertheless, the use of VAS parameterization provides the most accurate snow depth simulations for the alpine and tundra snowpacks.

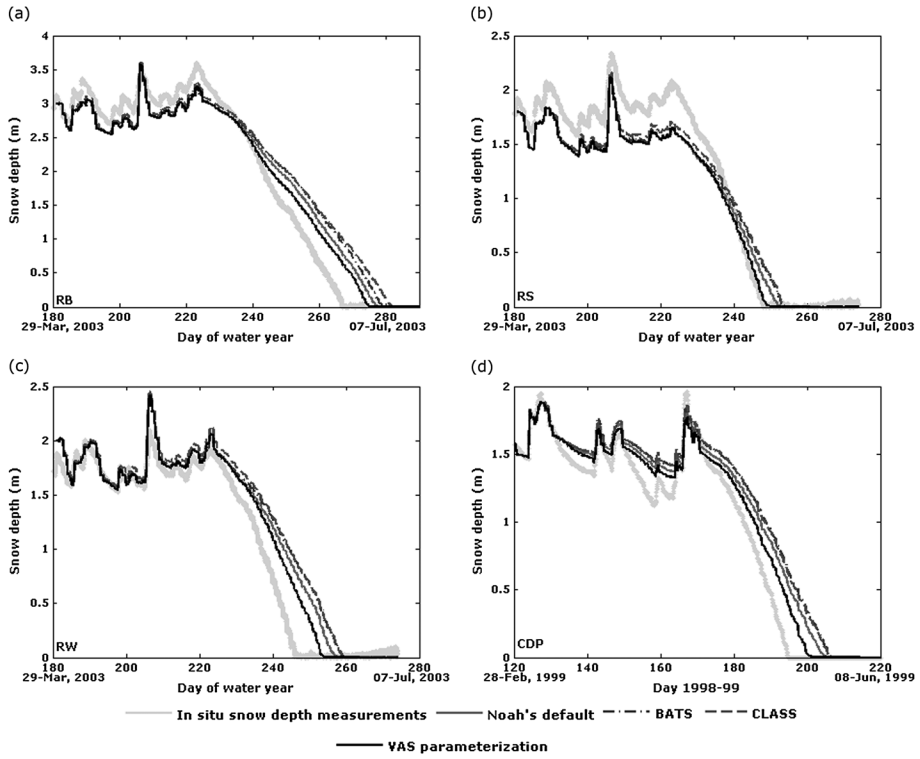

Figure 8. Time series of simulated and measured snow depths for alpine snow conditions: (a) RB site, (b) RS site, (c) RW site, and (d) CDP site.

A firm conclusion can, however, not be drawn for the prairie site (Figure 9b) because of the uncertainties involved in the applied precipitation as forcing and/or snowpack's density simulations.

It should, however, be noted that despite the superior error statistics, the improvements in snow depth simulations with the VAS parameterization are not statistically significant as compared to the other parameterizations. Further testing over longer periods and/or multiple sites is, therefore, required before a firm conclusion based on statistically significant results can be drawn. In addition, it should be noted that the albedo is only one component in the complex snow depletion process. A reduction of uncertainties in the snow density parameterization as well as the representation of wind effects on snow depth within model physics can further ameliorate the simulation of snow depletion, especially for the shallow tundra and prairie snowpacks. Updates to the snow density parameterization will have implications for simulations of the entire snow season, whereas improvements related to snow blowing may be limited for melt season because the presence of large snow grains and liquid water in snowpacks suppresses the wind effect.

6.3. Upward Shortwave Radiation

Figure 10 shows as an example measured and simulated upward shortwave radiation for the RB site for two periods: when the snowpack is melting (Figure 10a) and when the snowpack is ceasing to exist (Figure 10b).

Table 6. Error Statistics Computed Between Simulated and Measured Snow Depths for the Alpine Sites[a]

	Noah	BATS	CLASS	VAS
r	+0.957	+0.957	+0.947	+0.97
ME (m)	+0.05	+0.059	+0.107	+0.009
MAE (m)	0.203	0.2	0.227	0.169
RMSE (m)	0.264	0.263	0.302	0.217
p-value[b]	0.38	0.40	0.10	Reference

[a]Temporal autocorrelation is accounted for by averaging over the correlation length of 14 days, which resulted in a sample size of 30 averaged values.
[b]*p*-values are derived using the Wilcoxon test, which is more conservative than *t* test.

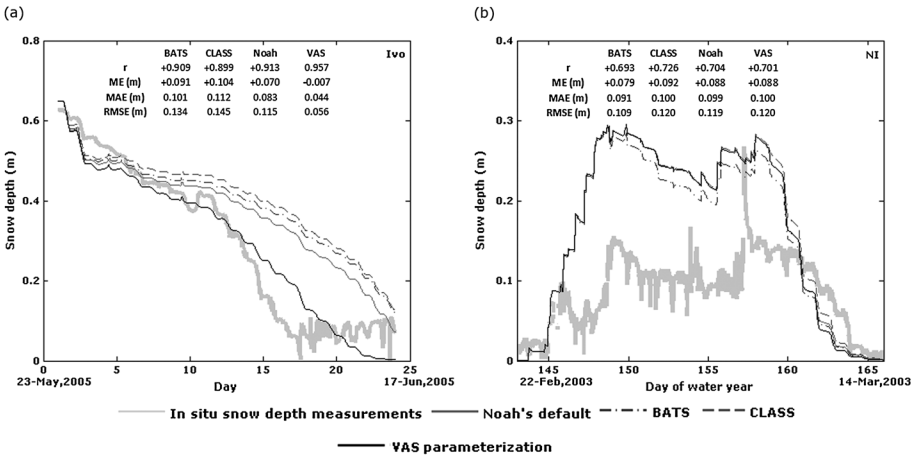

Figure 9. Time series of simulated and measured snow depths for tundra (Ivo) and prairie (NI) snow conditions: (a) Ivo site and (b) NI site.

Despite slight biases (overestimation) during melting, Figure 10a highlights that the VAS parameterization better reproduces the upward shortwave radiation than the other snow albedo parameterizations. These biases between the measurements and simulations, however, increase as the snowpack becomes optically thin (Figure 10b). Nevertheless, the VAS parameterization provides the best estimates of the upward shortwave radiation in comparison with the other albedo parameterizations. This behavior of upward shortwave radiation simulation, as noted in the figure, is representative of all the other alpine sites used in this study, which is confirmed by the error statistics given in Table 7. The reductions in the RMSE are, on average, 37%, 42%, and 26% when comparing the VAS simulations versus simulations with the BATS, CLASS, and Noah's default parameterizations, respectively.

6.4. Snowmelt

CDP is the only site in this study for which in situ snowmelt measurements are available, hence enables us to assess the simulated snowmelt against the measurements. All the four parameterizations produced

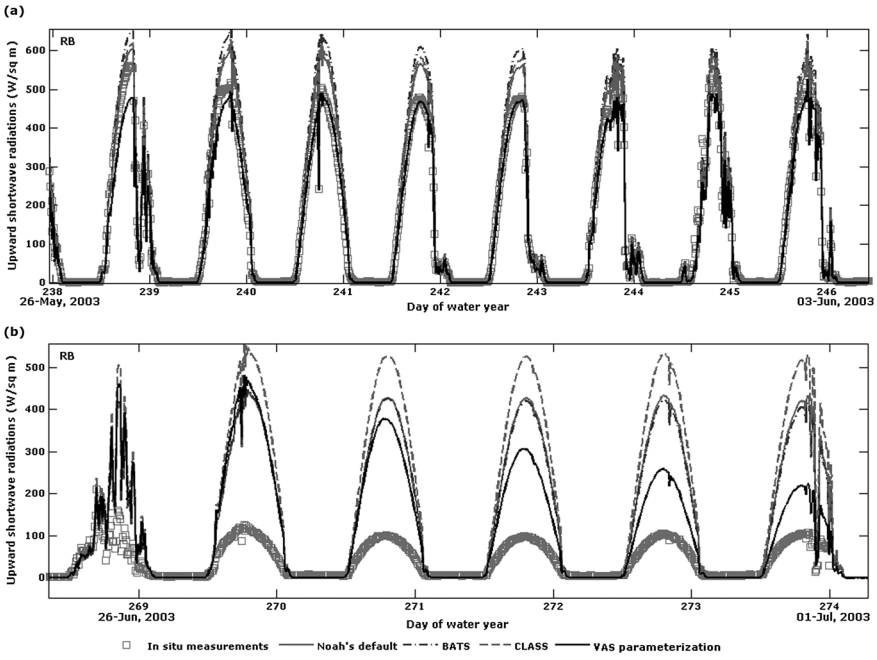

Figure 10. Measured and simulated upward shortwave radiative flux for the RB site. Figure 10a shows the period near the start of snow melting, and Figure 10b shows the period at the end of snow melting.

Table 7. Error Statistics Computed Between Measured Upward Shortwave Radiation Under Alpine Snow Conditions and Simulations With Four Snow Albedo Parameterizations

Snow Albedo Parameterizations			FA	RB	RS	RW
BATS	ME	W/m^2	+99.92	+44.10	+90.94	+61.08
	RMSE	W/m^2	135.12	97.06	120.55	122.94
CLASS	ME	W/m^2	+107.97	+70.06	+95.46	+69.81
	RMSE	W/m^2	136.40	135.02	121.44	124.18
Noah's default	ME	W/m^2	+68.96	+33.62	+79.61	+47.45
	RMSE	W/m^2	114.04	89.74	101.79	100.26
VAS	ME	W/m^2	+59.03	+15.26	+52.89	+16.70
	RMSE	W/m^2	88.11	71.46	80.97	59.77

intermittent spells of snowmelt during the melting period and very strong snow melting during the last melting spell, as observed during the 1999 spring (Figure 11a). The existing parameterizations simulate higher albedo and thus produce a lower snowmelt, which is amplified by the fact that Noah simulates a prolonged presence of a snowpack. Noah with the VAS parameterization produces a somewhat higher snowmelt and melts the snowpack completely close to the observed end of the melt season. The accumulation of snowmelt from its onset till the observed end is with the VAS parameterization 19%, 18%, and 12% higher than the BATS, CLASS, and Noah's default parameterization, respectively. Figure 11b shows comparison of the simulation with the measurements, which is quantified in Table 8. The achieved errors statistics suggest that all the parameterizations are capable of generating a good agreement with the observations (i.e., $r > 0.60$). However, Noah with the VAS parameterization simulates snowmelt rate and duration that agree better with the measurements. This will ultimately affect also the simulation of both energy and water budget components (i.e., streamflow). The performance of the snow albedo parameterizations for snowmelt simulations are further confirmed for the 2009 spring season (see Figure 11c and Table 8).

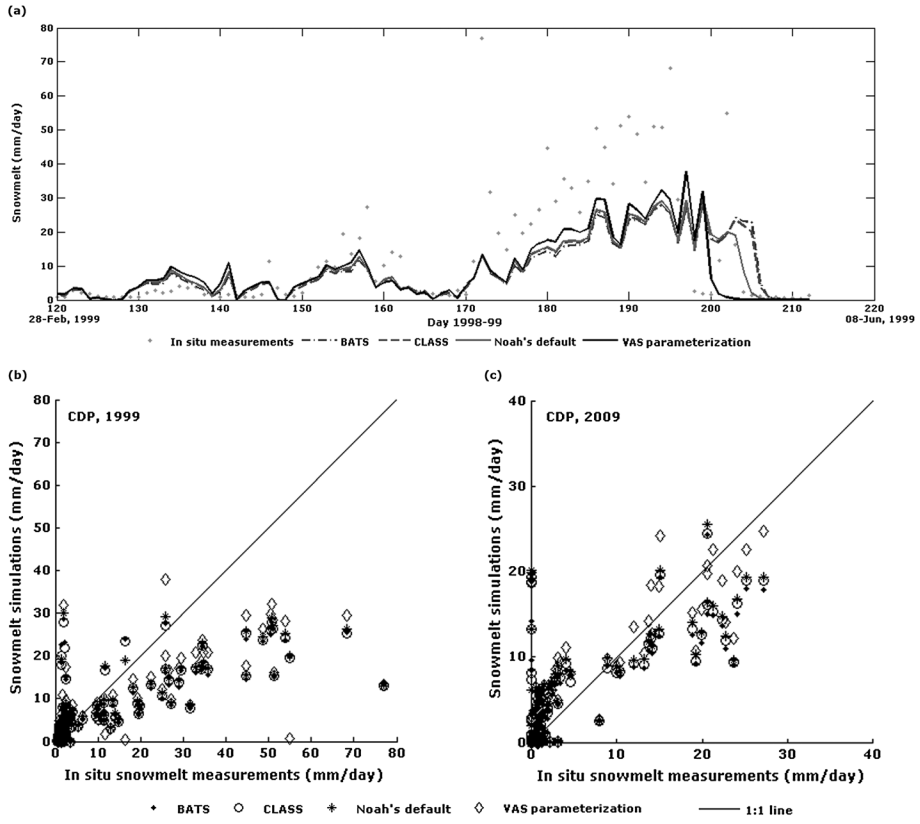

Figure 11. Snowmelt at the CDP site: measured and simulated. Figure 11a is the time series of the 1999 springtime. Figures 11b and 11c show scatterplots of simulations versus measurements of the 1999 and 2009 spring times, respectively.

Table 8. Statistics of Comparison Between Measured and Simulated Snowmelt for the CDP Site

		BATS	CLASS	Noah	VAS
			1999		
r		+0.64	+0.67	+0.71	+0.82
ME	mm/day	−4.45	−4.45	−4.46	−4.47
MAE	mm/day	9.36	9.12	8.65	7.26
RMSE	mm/day	14.68	14.39	13.88	12.22
			2009		
r		+0.68	+0.71	+0.75	+0.91
ME	mm/day	+0.62	+0.62	+0.62	+0.62
MAE	mm/day	4.03	3.76	3.52	2.41
RMSE	mm/day	5.99	5.70	5.33	3.52

7. Implications at Large Scale

In this section, we investigate the impact of snow albedo parameterizations on the land surface water budget at basin scale, specifically the runoff and evapotranspiration (ET). Implementations of the default and the VAS snow albedo parameterizations within the Noah model are deployed to perform the simulations for the Upper Colorado River Basin (UCRB). Runoff in the 279,300 km^2 sized basin is dominated by snowmelt with roughly 70% of its annual streamflow produced by snowpacks [*Christensen and Lettenmaier*, 2007]. Noah's default snow albedo parameterization is implemented in its standard form (i.e., $A = 0.94$ and $= 0.58$), and for the VAS parameterization, the dynamic range (a) is set to 22 days, and 0.45 is taken for the minimum snow albedo (c).

The Noah LSM is initialized using the outputs from the Phase 2 of the North American Land Data Assimilation System (NLDAS-2), which are essentially Noah simulations performed from 1 January 1979 to present with the same vegetation, soil, topographical parameters, and the atmospheric forcing data sets as used in the study. The NLDAS-2 atmospheric forcings are taken from the North American Regional Reanalysis, except precipitation. The NLDAS-2 precipitation is included from the National Centers for Environmental Prediction/Climate Prediction Center and temporally disaggregated to hourly, primarily using Stage II radar data and a combination of other observations, satellite retrievals, or model data when and where radar data are unavailable. Simulations are performed offline at a spatial resolution of 1/8° starting from 30 August 2008 till 30 September 2010, of which the 2009–2010 water year (October–September) is used for analysis. Hence, model initialization started 1 year before the analysis period and in a period of the year with little to no snow coverage.

The impact of the snow albedo parameterizations on snow coverage and snow cover duration is quantified, respectively, by spatially averaging snow cover fraction (SCF) for the entire basin and via the snow-covered days (SCD). The time series of this basin scale SCF (Figure 12a) shows that the snow covers nearly the entire UCRB before the onset of snowmelt and is almost completely melted at the end of June. This is also confirmed by the basin scale SCF derived from the 8 day Moderate Resolution Imaging Spectrometer (MODIS) product [*Hall et al*., 2006; *Salomonson and Appel*, 2004], which may underestimate snow cover in mountain-based areas when trees are present [*Arsenault et al*., 2014; *Rittger et al*., 2013]. It is noted that the difference in the snow coverage simulated with the two parameterizations starts from the onset of snowmelt and remains the entire snowmelt season. In comparison with the Noah's default snow albedo parameterization, the VAS parameterization generates a lower snow cover fraction (i.e., on average 0.025) during the spring season with the largest difference (i.e., 0.106) appearing at the middle of spring (i.e., end of March), when almost 50% of the snow cover has depleted. In comparison with the MODIS observations, Noah with both the parameterizations overestimates SCF. However, the overestimation with the VAS parameterization is about 70% (almost 2100 km^2 vs. 7200 km^2) lower than with the Noah's default snow albedo parameterization.

The SCD is calculated as the total number of days for which the snow cover fraction that Noah simulates for a grid cell is larger than 50% in accordance with previous studies [*Livneh et al*., 2010]. Figures 12b and 12c show, respectively, SCD simulated with the default and VAS parameterizations, and the SCD difference between the two simulations is shown in Figure 12d. The map shows the typical spatial snow distribution in

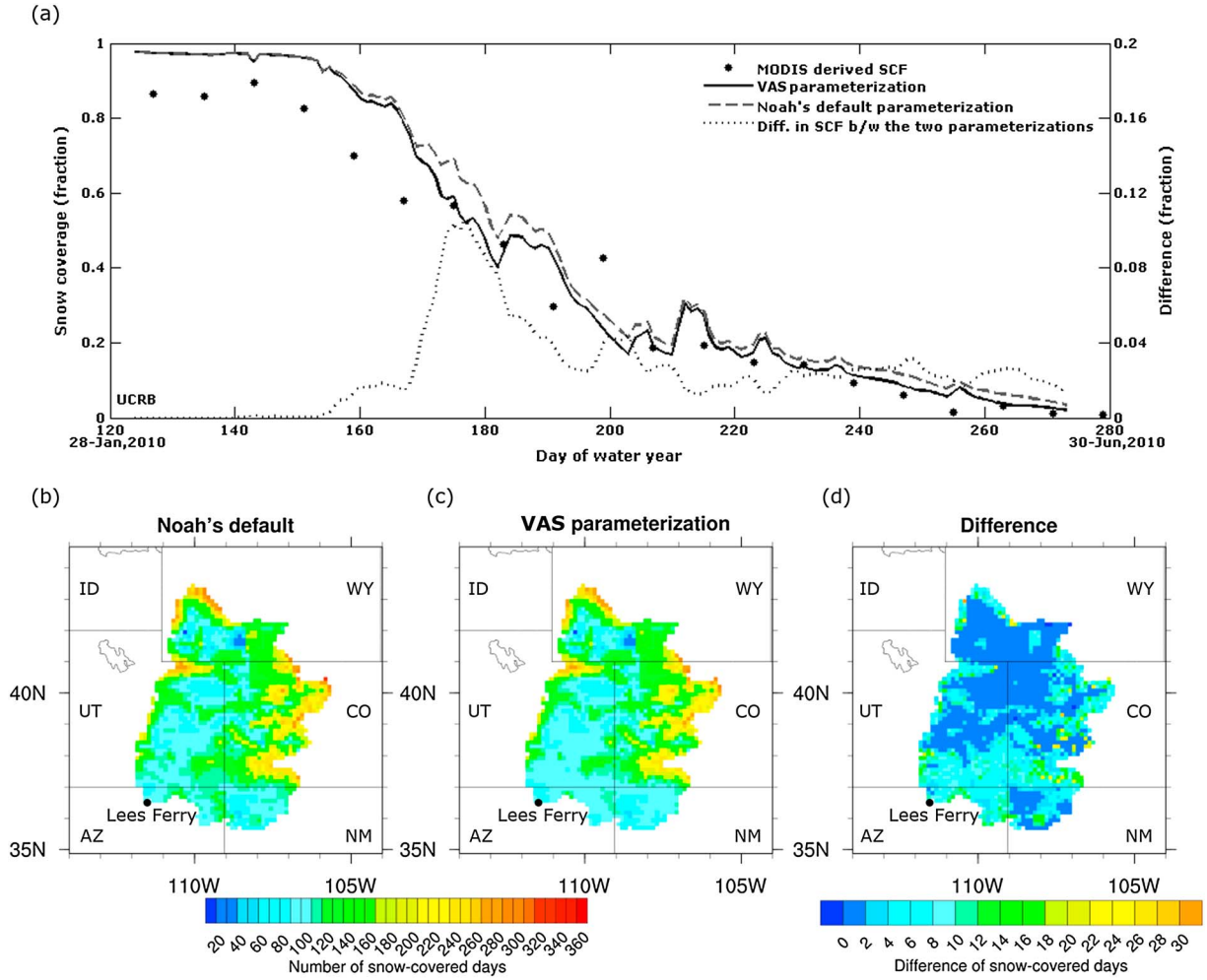

Figure 12. Noah simulated snow cover fraction (SCF) and snow-covered days (SCD) from 1 October 2009 to 30 September 2010 for the UCRB. Figure 12a shows time series of SCF simulated by Noah with the default and VAS parameterizations for snow albedo, SCF difference yielded with the two parameterizations, and SCF derived from 8 day MODIS snow cover product (MOD10A2). Figures 12b and 12c show the SCD simulated with the Noah's default and VAS parameterizations, respectively, and Figure 12d shows the difference [i.e., (b) minus (c)] between the SCD simulated by Noah with the two parameterizations.

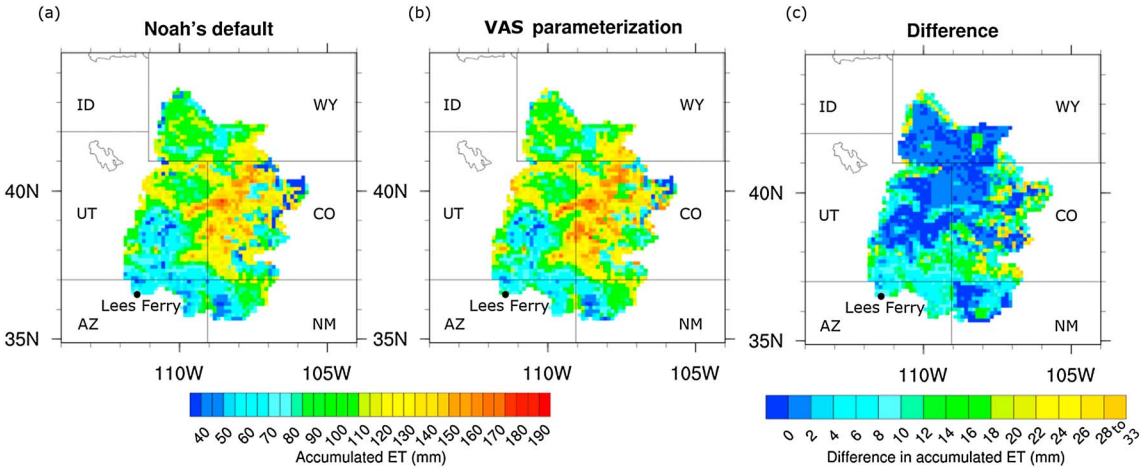

Figure 13. Noah simulated evapotranspiration (ET) for the Upper Colorado River Basin (UCRB). Figures 13a and 13b show accumulated ET produced, respectively, with the Noah's default and VAS parameterizations from 1 February to 30 June 2010; Figure 13c shows difference [i.e., (b) minus (a)] in the accumulated ET produced by Noah with the two parameterizations.

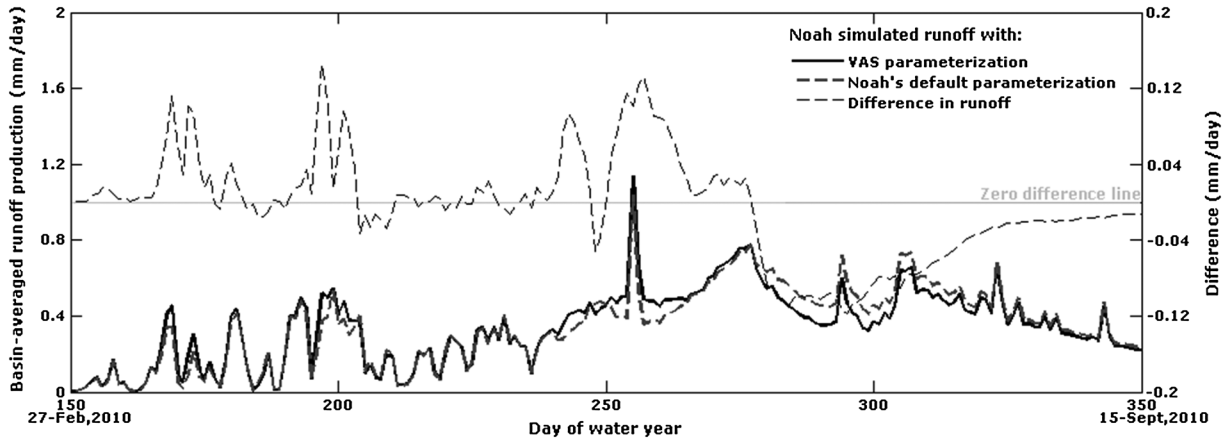

Figure 14. The Noah LSM simulated runoff (surface runoff + drainage) production with the VAS and default snow albedo parameterizations, and their difference. Values are averages across all basin grid cells (not routed flows).

the UCRB with an almost year-round snow coverage (>300 days) in the mountainous regions and around 60–100 days in the valleys. On average for the entire basin, the SCD decreases with the VAS parameterization by 4 days. However, over areas with deeper snowpacks (i.e., snow depth >1.0 m), the SCD decreases on average by 8 days with the VAS parameterization in comparison to the SCD with the Noah's default albedo parameterization. On the other hand, SCD difference is at most a day or a couple of days in valleys where snow accumulation is on average about 60 cm.

Besides the obvious impact on snow coverage and duration, the snow albedo parameterization also affects the simulated land surface water budgets (ET and runoff) in general. Figures 13a and 13b show the accumulated ET during springtime (i.e., 1 February 2010 to 30 June 2010) for the UCRB as a map using the default and VAS parameterizations, respectively, and Figure 13c displays the difference of the accumulated ET simulated with the two parameterizations. From the figures, it can be deduced that the VAS parameterization accumulates about 3 mm more ET than the Noah's default parameterization. For specific areas, however, the difference in accumulated ET can be on average as large as 8 mm over deeper snowpacks (i.e., snow depth >1.0 m).

The runoff generated by Noah with the default and VAS snow albedo parameterizations is determined by summing for each grid cell the total Noah runoff (viz. surface runoff and drainage). Figure 14 shows the time series of spatially averaged runoff production simulated by Noah with the VAS parameterization, with the default snow albedo parameterization as well as their difference. The peak differences between the runoff simulations with the default and VAS snow albedo parameterizations are noted during springtime, from March. With the VAS parameterization, Noah simulates initially larger runoff amounts which changes to smaller amounts as the melt season continues and snowpacks deplete. As such, it can be concluded that with the VAS parameterization Noah simulates a slightly higher and earlier runoff peak than the default simulation. Skill in reproducing peak runoffs becomes imperative in a changing climate and the forecasting extreme streamflows.

8. Conclusion

In this study, we examine observed snow albedo decay during springtime and assess the performance of the Noah, BATS, and CLASS land surface models (LSM) snow albedo parameterizations. The latter two parameterizations were implemented within the overall model physics of the Noah LSM. The Noah LSM was run using the three parameterizations across the snowmelt seasons characterized at seven sites, of which five are from alpine, one from tundra, and one from prairie snow conditions. The comparison of the simulated snow albedo evolution with the in situ measurements shows that the parameterizations adopted by Noah, BATS, and CLASS are only able to simulate an albedo decay but do not reproduce its stabilization at the minimum value of optically thick snowpacks within the observed time. This limitation directly affects the rate of the snow albedo decay and total range of simulated snow albedo values. At present, the above mentioned

parameterizations overestimate snow albedo during the melt season, which reduces the Noah simulated melt rate and extends the simulated snowpack duration.

Based upon these observations, we propose a new parameterization for simulating the snow albedo during the melting period that adopts the shape of a semi-variogram when the snowpack remains optically thick and decreases the albedo further via a weighted average of snow and land surface (background) albedos as a function of snow depth when the snowpack becomes optically thin. The variogram-shaped (VAS) snow albedo parameterization has been implemented in the Noah LSM and employed for simulating the snow processes over alpine, tundra, and prairie snowpacks. Apart from an improved snow albedo simulation, the VAS parameterization also has positive impacts on the simulation of snow depth, melt rate, snowpack duration, and upward shortwave radiation. Improvements obtained with the VAS parameterization consist essentially of a lower deep snowpack albedo for the melt season that accelerates the melt rate and associated surface hydrological processes.

In spite of these improvements, uncertainties still exist particularly during episodes with optically thin snowpacks (e.g., snow density, atmospheric forcings). These make the impact of the VAS parameterization on simulations for the shallow prairie snowpacks less notable. Therefore, further studies are required to optimize the snow albedo modeling for prairie snowpacks and, arguably, to improve the snow density parameterization.

The impact of the snow albedo is also assessed at a large scale for the Upper Colorado River Basin by comparing the Noah simulations with the VAS and default parameterizations. Noah simulates, in line with the results obtained at plot scale, with the VAS parameterization a shorter snowpack duration. Notably, the fractional snow coverage simulated with the VAS parameterization agrees better with the snow cover observed by MODIS. This difference in the simulation of the snowpack states increases the evapotranspiration during the selected spring season of 2010 and affects the timing and magnitude of the runoff production. Noah simulates with the VAS parameterization a higher runoff peak in springtime and smaller volumes in the summer season.

The improvement in snow albedo simulation with the VAS parameterization has demonstrated the potential to improve the simulation of the land-surface states, energy, and water fluxes at the land-atmosphere interface, which may also positively impact the simulation of atmospheric processes when operated in a coupled system. However, additional testing over longer periods (i.e., multiple snow seasons) at different spatial resolutions, climatic regions, and physiographic conditions (i.e., forest-covered areas) is required to draw firm conclusions about the impact of different snow albedo parameterizations in simulating the snowpack properties and to validate large-scale simulations. The VAS parameterization is numerically efficient, and its parameters are derived from albedo measurements, which can also be obtained via satellite observations. The latter is particularly relevant in view of the recent launch of Landsat-8 and the upcoming Sentinel-2 mission with its launch date scheduled in 2014.

Acknowledgments

This study was financially supported by the Higher Education Commission (HEC) of Pakistan and facilitated by NUFFIC (The Netherlands). We would like to thank the Cold Land Processes Field Experiment (CLPX) team for the data collection and the National Snow and Ice Data Center (NSIDC) for making these data sets available at http://nsidc.org/data/clpx/clpx_data.html. We also thank NOAA/NCEP and NASA/GSFC for NLDAS-2 forcing and model output data, which is freely available at http://www.emc.ncep.noaa.gov/mmb/nldas/ and http://disc.sci.gsfc.nasa.gov/hydrology/data-holdings. Further thanks go to the PANGAEA repository and Ameriflex for providing the data sets at http://doi.pangaea.de/10.1594/PANGAEA.774249 as well as on the public ftp server ftp://ftp-cnrm.meteo.fr/pub-cencdp/, and http://ameriflux.ornl.gov/, respectively. Finally, we thank the three anonymous reviewers for their valuable comments, which have considerably improved this article.

References

Allen, R. J., and C. S. Zender (2010), Effects of continental-scale snow albedo anomalies on the wintertime Arctic oscillation, *J. Geophys. Res.*, *115*, *D23105*, doi:10.1029/2010JD014490.

Anderson, E. A. (1976), A point energy and mass balance model of a snow cover, Office of Hydrology, National Weather Service, 150.

Arsenault, K. R., P. R. Houser, and G. J. M. De Lannoy (2014), Evaluation of the MODIS snow cover fraction product, *Hydrol. Processes*, *28*(3), 980–998, doi:10.1002/hyp.9636.

Barlage, M., F. Chen, M. Tewari, K. Ikeda, D. Gochis, J. Dudhia, R. Rasmussen, B. Livneh, M. Ek, and K. Mitchell (2010), Noah land surface model modifications to improve snowpack prediction in the Colorado Rocky Mountains, *J. Geophys. Res.*, *115*, D22101, doi:10.1029/2009JD013470.

Barnett, T. P., J. C. Adam, and D. P. Lettenmaier (2005), Potential impacts of a warming climate on water availability in snow-dominated regions, *Nature*, *438*(7066), 303–309, doi:10.1038/nature04141.

Broyden, C. G. (1970), The Convergence of a Class of Double-rank Minimization Algorithms 1. General Considerations, *IMA J. Appl. Math.*, *6*, 76–90, doi:10.1093/imamat/6.1.76.

Cherkauer, K. A., L. C. Bowling, and D. P. Lettenmaier (2003), Variable infiltration capacity cold land process model updates, *Global Planet. Change*, *38*(1–2), 151–159, doi:10.1016/S0921-8181(03)00025-0.

Christensen, N. S., and D. P. Lettenmaier (2007), A multimodel ensemble approach to assessment of climate change impacts on the hydrology and water resources of the Colorado River Basin, *Hydrol. Earth Syst. Sci.*, *11*(4), 1417–1434, doi:10.5194/hess-11-1417-2007.

Cline, D. W. (1997a), Snow surface energy exchanges and snowmelt at a continental, midlatitude Alpine site, *Water Resour. Res.*, *33*(4), 689–701, doi:10.1029/97WR00026.

Cline, D. W. (1997b), Effect of seasonality of snow accumulation and melt on snow surface energy exchanges at a continental Alpine site, *J. Appl. Meteorol.*, *36*(1), 32–51, doi:10.1175/1520-0450(1997)036<0032:EOSOSA>2.0.CO.

Dickinson, R. E., A. Henderson-Sellers, and P. J. Kennedy (1993), *Biosphere-Atmosphere Transfer Scheme (BATS) Version 1e as Coupled to the NCAR Community Climate Model*, *Tech. Note NCAR/TN-387+STR*, Natl. Cent. for Atmos. Res., Boulder, Colo.

Ek, M. B., K. E. Mitchell, Y. Lin, E. Rogers, P. Grunmann, V. Koren, G. Gayno, and J. D. Tarpley (2003), Implementation of Noah land surface model advances in the National Centers for Environmental Prediction operational mesoscale Eta model, *J. Geophys. Res.*, *108*(D22), 8851, doi:10.1029/2002JD003296.

Ek, M. B., et al. (2011), North American Land Data Assimilation System Phase 2 (NLDAS-2): Development and applications, GEWEX News, *21(2)*.

Elder, K., and A. Goodbody (2004), *CLPX-Ground: ISA Main Meteorological Data*, Natl. Snow and Ice Data Cent., Boulder, Colo. [Available at http://nsidc.org/data/nsidc-0172.html, accessed 4 December 2013.]

Elder, K., D. Cline, A. Goodbody, P. Houser, G. E. Liston, L. Mahrt, and N. Rutter (2009), NASA Cold Land Processes Experiment (CLPX 2002/03): Ground-Based and Near-Surface Meteorological Observations, *J. Hydrometeorol.*, *10*(1), 330–337, doi:10.1175/2008JHM878.1.

Feng, X., A. Sahoo, K. Arsenault, P. Houser, Y. Luo, and T. J. Troy (2008), The impact of snow model complexity at three CLPX sites, *J. Hydrometeorol.*, *9*(6), 1464–1481, doi:10.1175/2008JHM860.1.

Fletcher, C. G., S. C. Hardiman, P. J. Kushner, and J. Cohen (2009a), The dynamical response to snow cover perturbations in a large ensemble of atmospheric GCM integrations, *J. Clim.*, *22*(5), 1208–1222, doi:10.1175/2008JCLI2505.1.

Fletcher, C. G., P. J. Kushner, A. Hall, and X. Qu (2009b), Circulation responses to snow albedo feedback in climate change, *Geophys. Res. Lett.*, *36*, L09702, doi:10.1029/2009GL038011.

Fletcher, R. (1970), A new approach to variable metric algorithms, *Comput. J.*, *13*, 317–322, doi:10.1093/comjnl/13.3.317.

Goldfarb, D. (1970), A family of variable-metric methods derived by variational means, *Math. Comput.*, *24*, 23–26, doi:10.1090/S0025-5718-1970-0258249-6.

Hall, D. K., G. A. Riggs, and V. V. Salomonson (2006), *MODIS/Terra Snow Cover 8-day L3 Global 500 m Grid V005 (MODIS Snow Products User Guide to Collection 5)*, Natl. Snow and Ice Data Cent., Boulder, Colo.

Klein, A. G., and J. Stroeve (2002), Development and validation of a snow albedo algorithm for the MODIS instrument, *Ann. Glaciol.*, *34*(1), 45–52, doi:10.3189/172756402781817662.

Koivusalo, H., and H. Heikinheimo (1999), Surface energy exchange over a boreal snowpack: comparison of two snow energy balance models, *Hydrol. Processes*, *13*(14–15), 2395–2408, doi:10.1002/(SICI)1099-1085(199910)13:14/15<2395::AID-HYP864>3.0.CO;2-G.

Liang, S., J. Stroeve, and J. E. Box (2005), Mapping daily snow/ice shortwave broadband albedo from Moderate Resolution Imaging Spectroradiometer (MODIS): The improved direct retrieval algorithm and validation with Greenland in situ measurement, *J. Geophys. Res.*, *110*(D10), D10109, doi:10.1029/2004JD005493.

Livneh, B., Y. L. Xia, K. E. Mitchell, M. B. Ek, and D. P. Lettenmaier (2010), Noah LSM snow model diagnostics and enhancements, *J. Hydrometeorol.*, *11*(3), 721–738, doi:10.1175/2009JHM1174.1.

Lynch, A. H., D. L. McGinnis, and D. A. Bailey (1998), Snow-albedo feedback and the spring transition in a regional climate system model: Influence of land surface model, *J. Geophys. Res.*, *103*(D22), 29,037–29,049, doi:10.1029/98JD00790.

Malik, M. J., R. van der Velde, Z. Vekerdy, Z. Su, and M. F. Salman (2011), Semi-empirical approach for estimating broadband albedo of snow, *Remote Sens. Environ.*, *115*(8), 2086–2095, doi:10.1016/j.rse.2011.04.010.

Malik, M. J., R. van der Velde, Z. Vekerdy, and Z. Su (2012), Assimilation of satellite-observed snow albedo in a land surface model, *J. Hydrometeorol.*, *13*(3), 1119–1130, doi:10.1175/JHM-D-11-0125.1.

Marks, D., and J. Dozier (1992), Climate and energy exchange at the snow surface in the Alpine Region of the Sierra Nevada: 2. Snow cover energy balance, *Water Resour. Res.*, *28*(11), 3043–3054, doi:10.1029/92WR01483.

Marks, D., M. Reba, J. Pomeroy, T. Link, A. Winstral, G. Flerchinger, and K. Elder (2008), Comparing simulated and measured sensible and latent heat fluxes over snow under a pine canopy to improve an energy balance snowmelt model, *J. Hydrometeorol.*, *9*(6), 1506–1522, doi:10.1175/2008JHM874.1.

Meiman, J. R., E. Remmenga, and H. Keller (1971), Snow distribution in relation to solar radiation on two Swiss Pre-Alp watersheds, *Water Resour. Res.*, *7*(6), 1636–1640, doi:10.1029/WR007i006p01636.

Molotch, N. P., and R. C. Bales (2006), Comparison of ground-based and airborne snow surface albedo parameterizations in an alpine watershed: Impact on snowpack mass balance, *Water Resour. Res.*, *42*, W05410, doi:10.1029/2005WR004522.

Morin, S., Y. Lejeune, B. Lesaffre, J.-M. Panel, D. Poncet, P. David, and M. Sudul (2012), An 18-yr long (1993–2011) snow and meteorological dataset from a mid-altitude mountain site (Col de Porte, France, 1325 m alt.) for driving and evaluating snowpack models, *Earth Syst. Sci. Data*, *4*(1), doi:10.5194/essd-4-13-2012.

Oechel, W. C. (2012), Meteorological/Flux measurements at Ivotuk / US-Ivo, *AmeriFlux Site and Data Exploration System*. [Available at http://ameriflux.ornl.gov/fullsiteinfo.php?sid=20, accessed 4 December 2013.]

Pan, M., et al. (2003), Snow process modeling in the North American Land Data Assimilation System (NLDAS): 2. Evaluation of model simulated snow water equivalent, *J. Geophys. Res.*, *108*(D22), 8850, doi:10.1029/2003JD003994.

Picard, G., F. Domine, G. Krinner, L. Arnaud, and E. Lefebvre (2012), Inhibition of the positive snow-albedo feedback by precipitation in interior Antarctica, *Nat. Clim. Change*, *2*(11), 795–798, doi:10.1038/nclimate1590.

Qu, X., and A. Hall (2006), Assessing snow albedo feedback in simulated climate change, *J. Clim.*, *19*(11), 2617–2630, doi:10.1175/JCLI3750.1.

Randall, D. A., et al. (1994), Analysis of snow feedbacks in 14 general circulation models, *J. Geophys. Res.*, *99*(D10), 20,757–20,771, doi:10.1029/94JD01633.

Rittger, K., T. H. Painter, and J. Dozier (2013), Assessment of methods for mapping snow cover from MODIS, *Adv. Water Resour.*, *51*(0), 367–380, doi:10.1016/j.advwatres.2012.03.002.

Salomonson, V. V., and I. Appel (2004), Estimating fractional snow cover from MODIS using the normalized difference snow index, *Remote Sens. Environ.*, *89*(3), 351–360, doi:10.1016/j.rse.2003.10.016.

Shanno, D. F. (1970), Conditioning of Quasi-Newton methods for function minimization, *Math. Comput.*, *24*, 647–656, doi:10.1090/S0025-5718-1970-0274029-X.

Sheffield, J., et al. (2003), Snow process modeling in the North American Land Data Assimilation System (NLDAS): 1. Evaluation of model-simulated snow cover extent, *J. Geophys. Res.*, *108*(D22), 8849, doi:10.1029/2002JD003274.

Souma, K., and Y. Q. Wang (2010), A comparison between the effects of snow albedo and infiltration of melting water of Eurasian snow on East Asian summer monsoon rainfall, *J. Geophys. Res.*, *115*, D02115, doi:10.1029/2009JD012189.

Sturm, M., J. Holmgren, and G. E. Liston (1995), A seasonal snow cover classification system for local to global applications, *J. Clim.*, *8*(5), 1261–1283, doi:10.1175/1520-0442(1995)008<1261:ASSCCS>2.0.CO;2.

U.S. Army Corps Of Engineers (1956), Snow hydrology: Summary report of the snow investigations, U. S. Army of Engineers North Pacific Division.

Verseghy, D. L. (1991), Class—A Canadian land surface scheme for GCMS. I. Soil model, *Int. J. Climatol.*, *11*(2), 111–133, doi:10.1002/joc.3370110202.

Wigmosta, M. S., L. W. Vail, and D. P. Lettenmaier (1994), A distributed hydrology-vegetation model for complex terrain, *Water Resour. Res.*, *30*(6), 1665–1679, doi:10.1029/94WR00436.

Wiscombe, W. J., and S. G. Warren (1980), A model for the spectral albedo of snow. 1. Pure snow, *J. Atmos. Sci.*, *37*(12), 2712–2733, doi:10.1175/1520-0469(1980)037<2712:AMFTSA>2.0.CO;2.

Xia, Y. L., M. Ek, H. L. Wei, and J. Meng (2012), Comparative analysis of relationships between NLDAS-2 forcings and model outputs, *Hydrol. Processes*, *26*(3), 467–474, doi:10.1002/hyp.8240.

Xue, Y., S. Sun, D. S. Kahan, and Y. Jiao (2003), Impact of parameterizations in snow physics and interface processes on the simulation of snow cover and runoff at several cold region sites, *J. Geophys. Res.*, *108*(D22), 8859, doi:10.1029/2002JD003174.

Zender, C. S. (2012), Cryoscience: Snowfall brightens Antarctic future, *Nat. Clim. Change*, *2*(11), 770–771, doi:10.1038/nclimate1730.